HOSTED BY
ELSEVIER
CrossMark
Available online at www.sciencedirect.com
ScienceDirect
Defence Technology 11 (2015) 330–337
www.elsevier.com/locate/dt

Optimization of friction stir welding parameters for improved corrosion resistance of AA2219 aluminum alloy joints

G. RAMBABU [a], D. BALAJI NAIK [a], C.H. VENKATA RAO [b], K. SRINIVASA RAO [b,*], G. MADHUSUDAN REDDY [c]

[a] *Department of Mechanical Engineering, Andhra University, Visakhapatnam, India*
[b] *Department of Metallurgical Engineering, Andhra University, Visakhapatnam, India*
[c] *Defence Metallurgical Research Laboratory, Hyderabad, India*

Received 18 March 2015; revised 23 April 2015; accepted 7 May 2015
Available online 29 May 2015

Abstract

The aluminium alloy AA2219 (Al−Cu−Mg alloy) is widely used in the fabrication of lightweight structures with high strength-to-weight ratio and good corrosion resistance. Welding is main fabrication method of AA2219 alloy for manufacturing various engineering components. Friction stir welding (FSW) is a recently developed solid state welding process to overcome the problems encountered in fusion welding. This process uses a non-consumable tool to generate frictional heat on the abutting surfaces. The welding parameters, such as tool pin profile, rotational speed, welding speed and axial force, play major role in determining the microstructure and corrosion resistance of welded joint. The main objective of this work is to develop a mathematical model to predict the corrosion resistance of friction stir welded AA2219 aluminium alloy by incorporating FSW process parameters. In this work a central composite design with four factors and five levels has been used to minimize the experimental conditions. Dynamic polarization testing was carried out to determine critical pitting potential in millivolt, which is a criteria for measuring corrosion resistance and the data was used in model. Further the response surface method (RSM) was used to develop the model. The developed mathematical model was optimized using the simulated annealing algorithm optimizing technique to maximize the corrosion resistance of the friction stir welded AA2219 aluminium alloy joints.

Keywords: AA2219 alloy; Friction stir welding; Rotational speed; Welding speed; Axial force; Tool pin profile; Corrosion resistance; Design of experiments; Simulated annealing algorithm

1. Introduction

Friction stir welding (FSW), an innovative solid state welding technique, is finding greater use in defence and aerospace applications [1]. This environment-friendly and energy-efficient technique can be used to join high strength aluminum alloys and other metallic materials that are difficult to be joined using the conventional fusion welding processes. In FSW, a rotating tool is forced down into the joint line under the conditions where the frictional heating is sufficient to cause a local increase in the temperature of the material to the range where it is readily deformed plastically [2]. Despite the evolution of numerous models and investigations, the flow of material is not fully understood [3]. The tool used in FSW has two distinct parts, the shoulder and the pin, and is designed to serve three functions: (i) generate the frictional or deformational heat that softens the work material around and ahead of the pin, (ii) control the material flow to produce a defect-free joint, and (iii) confine the hot material under the shoulder. Understanding the material flow is critical for determining the

* Corresponding author.
E-mail addresses: balajinayak278@gmail.com (D. BALAJI NAIK), arunaraok@yahoo.com (K. SRINIVASA RAO), gmreddy_dmrl@yahoo.com (G. MADHUSUDAN REDDY).
Peer review under responsibility of China Ordnance Society.

http://dx.doi.org/10.1016/j.dt.2015.05.003

accurate thermo-mechanical processing conditions during FSW. However, the material flow that occurs during the traverse of the rotating tool is reported to be chaotic and poorly understood [4]. Material flow analysis is important in developing a physical understanding of the mechanics of weld formation, which in turn is essential to manipulate the process parameters and produce the defect-free welds. Despite the fact that friction stir welded joints are now employed in a wide range of applications [5–12], many of the factors that control their microstructure and properties are still poorly understood, due to the complex nature of the metal-flow during welding. In addition to the process parameters, the effectiveness of the weld joint is strongly dependent on the geometric features of the tool. For instance, the height and shape of the pin [13–16], together with the shoulder diameter, exercise substantial influence on both the material-flow and heat generation caused by friction as well as rapid plastic deformation [17].

Extensive work on the influence of pin geometry on mechanical properties of 2014 aluminium alloy friction stir welds has been carried out by Zhao et al. [18]. Taper screw thread pin weld was reported to have the highest weld joint efficiency (75%) compared to the threaded cylindrical tool pin profile welds. The tools have all along been designed predominantly by the trial-and-error approach [19]. Most of the previous investigations on the design of tool geometry were focused on optimizing the tool pin profile with respect to microstructure and mechanical properties. However, the study did not provide any clear guidelines for the optimal design of tool geometry. While the effect of different pin profiles has been studied, very little effort has been made to study the influence of tool pin profile on the generation of heat during welding. Several studies concerning the calculation of thermal loading during FSW process are available in literature. Some of these studies [20,21] are based on the critical assumption that the heat generated due to pin-material interaction is very low compared to that generated by the shoulder and hence may be neglected. The influence of tool pin profiles on FSW was hardly discussed in the published literature.

In many industrial applications steels are readily replaced by nonferrous alloys and aluminium alloys. Some of these materials combine mechanical strength comparable with that of structural steels and low weight. While production of aluminium alloy component is not very complex, joining of these materials can sometimes cause serious problems. The friction stir welding, as a solid state joining technique, can be used to settle the problems appearing in joining of these materials, in which the joined material is plasticized by heat generated by friction between the surface of the plate and the contact surface of a special tool. The tool is composed of two main parts: shoulder and pin. The shoulder is responsible for generating the heat and containing the plasticized material in the weld zone, while the pin mixes the material of the components to be welded, thus creating a joint. This allows for producing defect-free welds characterized by good mechanical properties. However, the material flow behaviour is predominantly influenced by the FSW tool profiles, FSW tool dimensions and FSW process parameters [22].

In order to get the maximum corrosion resistance, FSW process parameters should be optimized. Tool pin profile plays a crucial role in material flow and, in turn, regulates the welding parameters of the FSW process [23]. Friction stir welds are characterized by well defined weld nugget and flow contours, almost spherical in shape, and these contours are dependent on the tool design, the welding parameters and the process conditions [24]. Hence, an attempt has been made to optimize the FSW process parameters to maximize the corrosion resistance of AA2219 aluminium alloy joints using the design of experiment concept, the response surface method and the simulated annealing algorithm.

2. Experimental details

2.1. Material and methods

In the present investigation, 240 mm × 160 mm × 7 mm rolled plates of high-strength aluminium–copper alloy AA2219-T87 were used for friction stir welding experiments. The chemical composition of the parent metal is given in Table 1. The plates were welded in a single pass, using the conical, square, triangle, pentagon and Hexagon pin profile tools (Fig. 1) on position controlled friction stir welding machine. Fig. 2 shows the weld beads of FS welds of five tool profiles. Keller's reagent is used for etching the polished surfaces and optical micrographs are recorded.

2.2. Pitting corrosion test

A software based GillAC electrochemical system was used for potentio-dynamic polarization tests to study the pitting corrosion behavior of the metal. A saturated calomel electrode (SCE) and platinum electrodes were used as reference and auxiliary electrodes respectively. All experiments were conducted in aerated 3.5% NaCl solutions with pH adjusted to 10 by adding potassium hydroxide. The potential scan was carried out at 0.166. The exposure area for these experiments was 1 cm^2. The potential at which current increased drastically was considered to be the critical pitting corrosion potential. The specimens exhibiting relatively more positive potential (or less negative potentials) were considered to have better pitting corrosion resistance.

2.3. Design of experiment

It is very difficult to form a mathematical equation for higher corrosion resistance values so for that we consider the ranges of friction stir parameters. The important factors influencing the corrosion properties of FSW joints and the working ranges of those factors for AA2219 aluminium alloy

Table 1
Chemical composition of AA2219 alloy.

Element	Cu	Mn	Zr	Si	Fe	Al
Wt.%	6.7	0.3	0.07	0.10	0.14	Bal

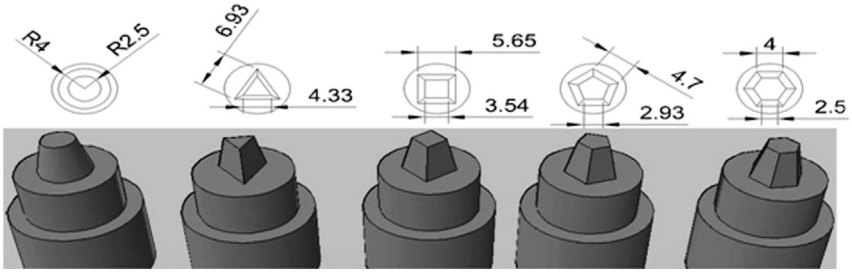

Fig. 1. Geometry of tool profiles.

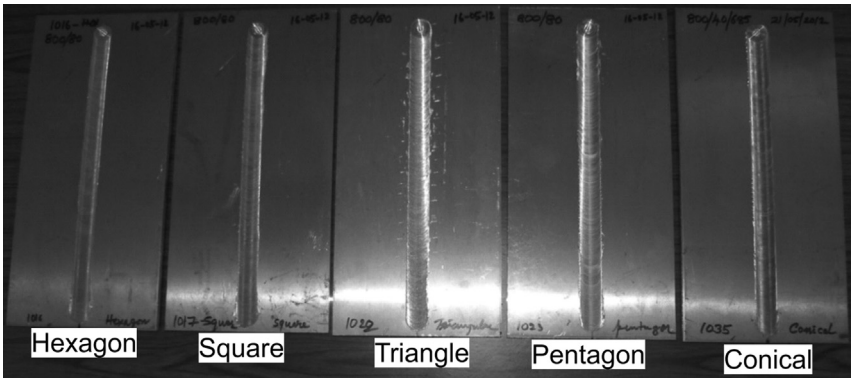

Fig. 2. Weld beads of FS welds of five profiles.

are presented in Table 2. Due to the wide range of influential factors, it was decided to use four factors, five levels, and a central composite design matrix to prescribe the required number of experiment.

Table 3 shows the 31 sets of coded conditions used to form the design matrix. The data in Table 3 is used as input data to form a mathematical equation by the design of experiment method and response surface methodology in Mini-tab software.

2.4. Development of a mathematical model

The response function corrosion resistance (CR) of the joints is a function of the tool profile (P), rotational speed (N), welding speed (S) and axial force (F). It can be expressed as

$$CR = f(P, N, S, F) \tag{1}$$

The second order polynomial (regression) equation used to represent the response surface 'Y' is given by [25]

$$Y = b_0 + \sum b_i x_i + \sum b_{ii} x_2 + \sum b x_i x_j \tag{2}$$

And for four factors, the selected polynomial can be expressed as

$$\begin{aligned} CR = {} & b_0 + b_1(P) + b_2(N) + b_3(S) + b_4(F) + b_{11}(P_2) \\ & + b_{22}(N_2) + b_{33}(S_2) + b_{44}(F_2) + b_{12}(\mathrm{PN}) + b_{13}(\mathrm{PS}) \\ & + b_{14}(\mathrm{PF}) + b_{23}(\mathrm{NS}) + b_{24}(\mathrm{NF}) + b_{34}(\mathrm{SF}) \end{aligned} \tag{3}$$

where b_0 is the average of responses; and b_1, b_2, … , b_{23} are the coefficients which depend on the respective main and interaction effects of the parameters. All the coefficients were evaluated and tested for their significance at a 95% confidence level by applying a Minitab software package. The final mathematical model developed to predict corrosion rate of FSW joints of AA2219 aluminium alloy is given below

Table 2
Important factors and their levels.

S. No	Parameter	Notation	Unit	Levels				
				(−2)	(−1)	(0)	(+1)	(+2)
1	Tool profile	P	–	Hexagon	Pentagon	Square	Conical	Triangular
2	Rotational speed	N	RPM	1000	1100	1200	1300	1400
3	Welding speed	S	($\mathrm{mm \cdot min^{-1}}$)	600	700	800	900	1000
4	Axial force	F	kN	8	10	12	14	16

Table 3
Design matrix and experimental results.

Experiment number	Factor				Corrosion pit potential/mV
	P	N	S	F	
1	−1	−1	−1	−1	−572
2	+1	−1	−1	−1	−591
3	−1	+1	−1	−1	−577
4	+1	+1	−1	−1	−594
5	−1	−1	+1	−1	−575
6	+1	−1	+1	−1	−587
7	−1	+1	+1	−1	−568
8	+1	+1	+1	−1	−589
9	−1	−1	−1	+1	−569
10	+1	−1	−1	+1	−592
11	−1	+1	−1	+1	−574
12	+1	+1	−1	+1	−588
13	−1	−1	+1	+1	−573
14	+1	−1	+1	+1	−593
15	−1	+1	+1	+1	−576
16	+1	+1	+1	+1	−558
17	−2	0	0	0	−554
18	+2	0	0	0	−615
19	0	−2	0	0	−557
20	0	+2	0	0	−610
21	0	0	−2	0	−551
22	0	0	+2	0	−611
23	0	0	0	−2	−558
24	0	0	0	+2	−618
25	0	0	0	0	−586
26	0	0	0	0	−590
27	0	0	0	0	−582
28	0	0	0	0	−581
29	0	0	0	0	−591
30	0	0	0	0	−588
31	0	0	0	0	−587

$$CR = \{ -586.4286 - 9.5833P - 3.2500N - 3.4167S - 3.7500F + 1.232P^2 + 1.4821N^2 + 2.1071S^2 + 0.3571F^2 + 2.3750PS + 1.8750PF + 0.5000SF \} \quad (4)$$

The determination coefficient 'r_2' is used to find how close the predicted and experimental values lie [26]. The determination coefficient (r_2) indicates the goodness of fit for the model. In this case, the value of the determination coefficient ($r_2 = 0.92$) indicates that only less than 8% of the total variations are not explained by the model. The value of 'r_2' for the above-developed model is presented. This indicates that a high correlation exists among the experimental values and the predicted values. The normal probability plot for corrosion rate reveals that the residuals are falling on the straight line, which means the errors are distributed normally. All of this indicates an excellent suitability of the regression model (Fig. 5).

2.5. Contour plots and response graphs

Contour plots show a distinctive circular mound shape indicative of possible independence of factors on response. A contour plot was generated to visually display the region of optimal factor settings. For second-order response surfaces, such a plot can be more complex than the simple series of parallel lines that can occur with first-order models. Once a stationary point is found, it is usually necessary to characterize the response surface in the immediate vicinity of the point. Characterization is to identify whether the stationary point found is a maximum response, a minimum response or a saddle point. To classify this, the most straight-forward way is to examine through a contour plot. Contour plots play a very important role in the study of the response surface. By generating the contour plots using software for response surface analysis, the optimum can be located with reasonable accuracy by characterizing the shape of the surface. If a contour patterning of circular shaped contours occurs, it tends to suggest the independence of factor effects, while elliptical contours may indicate factor interactions [27]. Response surfaces have been developed for the proposed model, taking two parameters in the middle level and two parameters in 'X' and 'Y' axes as well as the response in 'Z' axis. The response surfaces clearly indicate an optimal response point.

3. Optimization of friction stir welding parameters

The traditional simulated annealing algorithm method [28] is used as an optimization tool to search the optimum values of the process variables. The mathematical model was framed by using the coded values. Hence, the coded values was optimized and then converted to the actual values. A computer program using MATLAB for the algorithm was developed to optimize the process variables. The objective is first written as a non-linear programming problem, (NLPP).

$$\text{Maximize } f\ (\text{response}) = f(P,N,S,F)$$
$$-2 \le P \le 2$$
$$-2 \le N \le 2$$

Variable bounds
$$-2 \le S \le 2$$
$$-2 \le F \le 2$$

3.1. Simulated annealing algorithm method

For a minimization problem with solution space S, objective function f and neighborhood structure N (Table 4):

Step 1: Select an initial solution S_0 and $S^* = S_0$, initial temperature $T > 0$,
Select a temperature reduction function α (T),

Table 4
Optimized friction stir welding parameters.

S. No	Parameter	Optimized value	Corrosion rate
1	Tool profile (P)	HEXAGON	−604.52
2	Rotational speed (N)/rpm	1307	
3	Welding speed (s)/(mm·min^{-1})	880.50	
4	Axial force (F)/kN	12.20	

Select a maximum iteration count Max; Repeat;
Step 2: Set iteration count $I\,T = 0$,
Repeat
$I\,T = I\,T + 1$
Step 3: Randomly; select $s \in N\,(S_0)$,
Set $\delta = f\,(s) - f\,(s_0)$;
Step 4: If $\delta < 0$,
Then set $s_0 = s$ (downhill move),
Else
Generate random x uniformly in the range [0, 1]; If $x <$ exp $(-\delta/T)$,
Then set $S_0 = S$ (uphill move) If $f\,(S_0) < f\,(S^*)$ then $S^* = S_0$
Until $I\,T =$ Max,
Set $T = \alpha\,(T)$,
Until stopping condition becomes true.
Output s^* as an approximation to the optimal solution.

4. Result and discussion

4.1. Microstructure of weld nugget zone

The weld nugget is formed where the tool pin penetrates the joint. It consists of recrystallized microstructure of very fine grains, as a result of the severe plastic deformation and high temperature. “Onion rings” are observed here, in the weld direction. It has been postulated that each rotation of the tool during FSW process results in extrusion of semi-cylinder layers of material, which displays the familiar onion ring structure when it is viewed from a sliced cross-section. Fig. 6 shows the microstructures in weld nugget zones welded by five different tools. The widths of nugget zone are 22 mm, 23 mm, 23 mm, 24 mm and 24 mm, respectively, for conical, square, triangle, pentagon and hexagon tools. A slight variation in width of weld nugget is observed this is due to heat generation during friction stir welding. The nugget region has experienced high temperatures and extensive plastic deformation, and is characterized by dynamically recrystallized grains. The deformation extent of the plastic material and the flow of the material are related to the microstructures and the properties of the nugget. Fine grain structure was acquired in the nugget zone. The size of the grain is bigger, and the grain boundaries distributions are uneven. The pin geometry affects the Nugget microstructures greatly. Definite change in weld made with hexagon tool was observed. The grains in the nugget region experienced high temperatures and turbulent material flow resulting in severe plastic deformation. Very fine grains are formed due to dynamically re-crystallization compared to weld nugget made with other tools (Fig. 6a–f). Specifically weld made with hexagon tool profile (Fig. 6(f)) shown very fine grain distribution compared to other tool profiles. From microstructural changes and results of weld nugget width it is clearly shown that the shape of the weld nugget zone is dependent on the tool shape, the tool geometry and the welding parameters.

The typical potentio-dynamic polarization curves of the weld nuggets of tool profile are given in Fig. 7, where the intermetallics are the initiation sites for pitting in Al–Cu alloys. The pitting is caused by the local dissolution of the

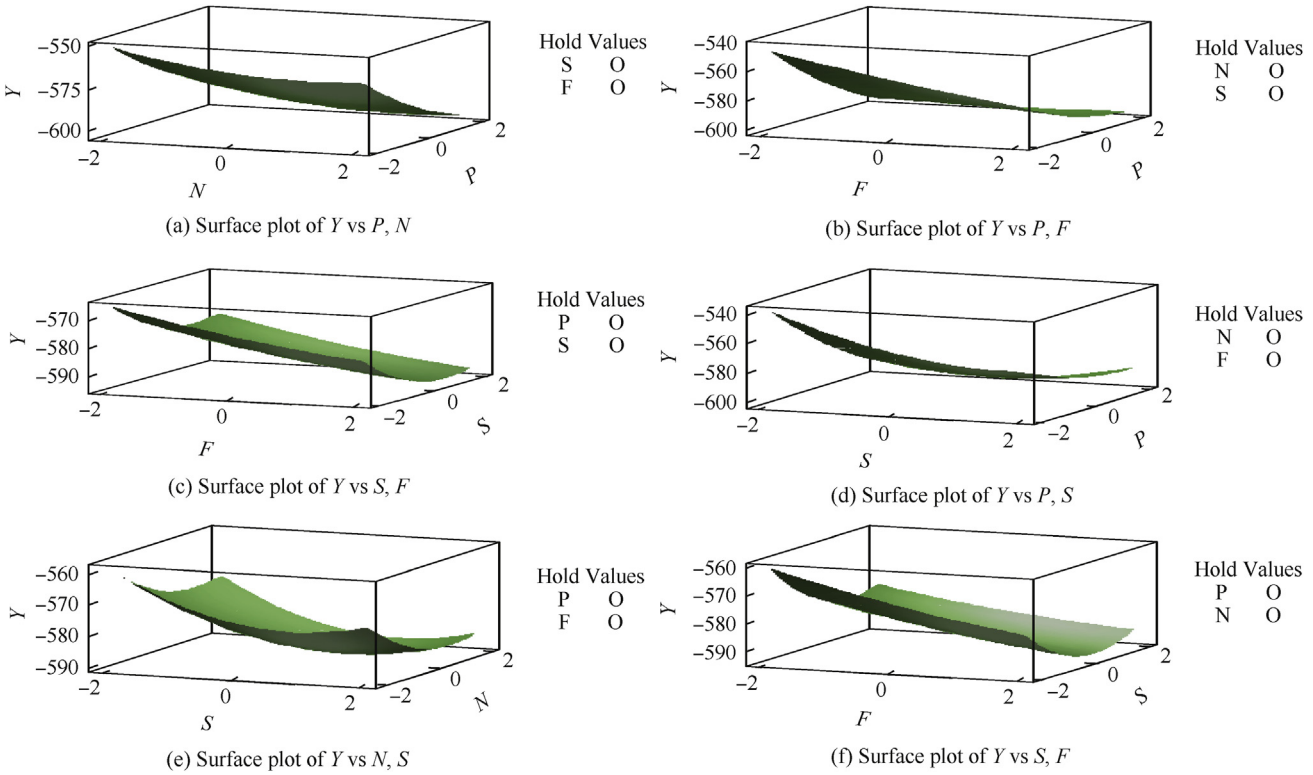

(a) Surface plot of Y vs P, N
(b) Surface plot of Y vs P, F
(c) Surface plot of Y vs S, F
(d) Surface plot of Y vs P, S
(e) Surface plot of Y vs N, S
(f) Surface plot of Y vs S, F

Fig. 3. Response graphs.

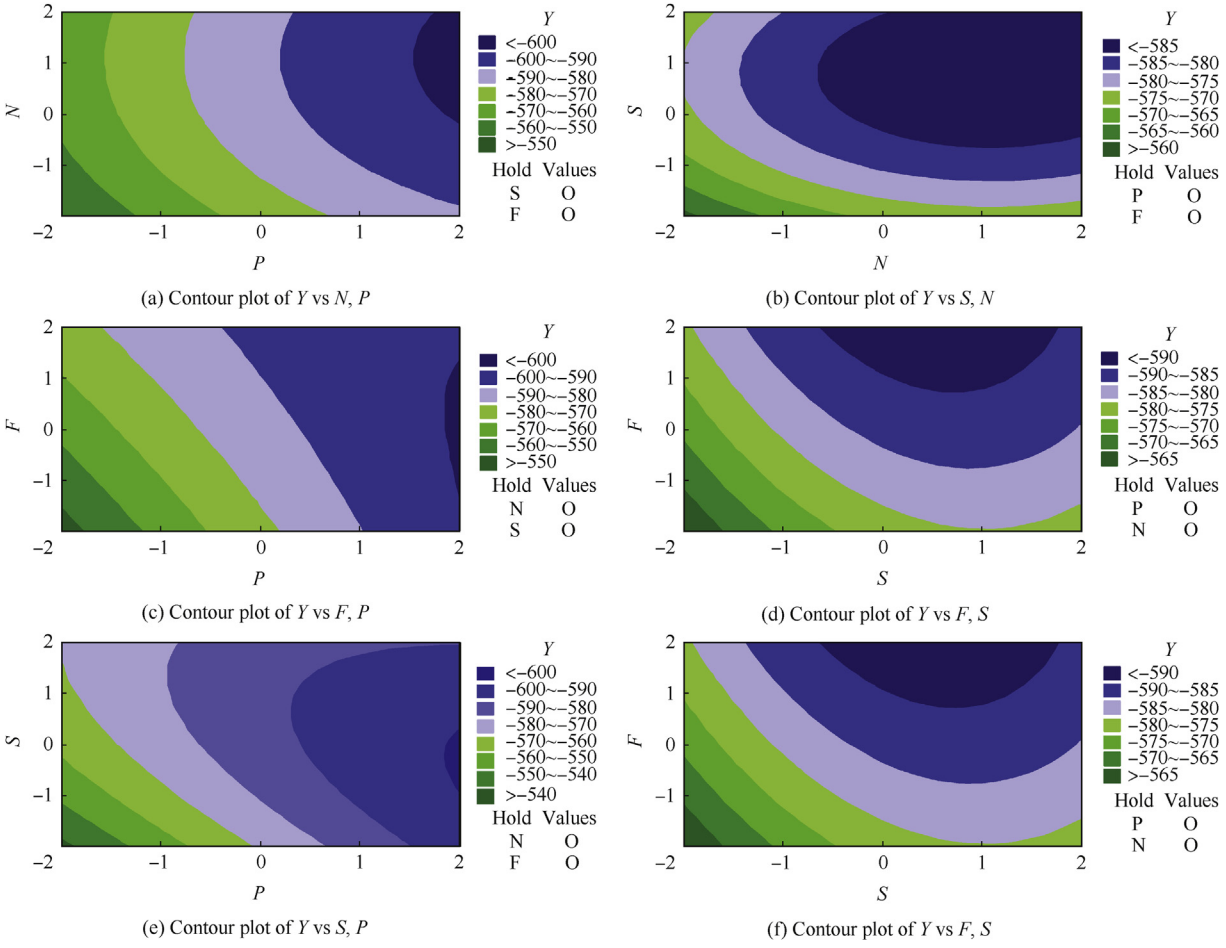

Fig. 4. Contour plots.

matrix due to galvanic coupling between intermetallics and surrounding matrix. From E_{pit} values (mV) of nugget zone (NZ) it is clearly noticed that the relatively more positive E_{pit} values are recorded in the NZ of the friction stir weld of hexagon tool profile. This is attributed to the dissolution/coarsening of the strengthening precipitates finely and evenly distributed in the nugget region of the hexagon profile. Since due to more heat is generated during FS welding, the corrosion behaviour of nugget zone is nobler compared to base metal due to absence of second phase particles, which is more clearly seen from Fig. 7 and the critical potential data.

From the experimental results, it is found that the joints fabricated using a hexagon pin profile tool with a rotational speed of 1300 rpm, a welding speed of 880 mm/min and an axial force of 12 KN exhibit the corrosion properties superior to those of the other joints. The reasons for the superior performance of such joints are explained below.

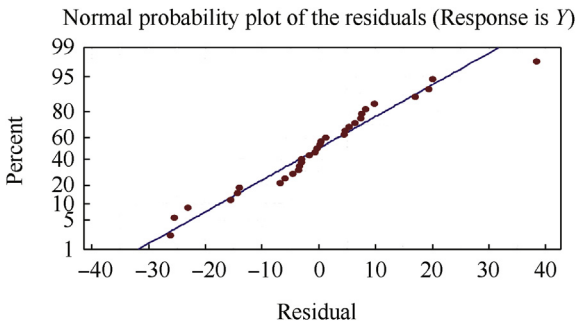

Fig. 5. Normal probability plot.

4.2. Analysis of response surface plots and contour plots

Fig. 3(a)–(f) presents three-dimensional responsive surface plots for the response corrosion resistance obtained from the regression model. The optimum corrosion rate is exhibited by the apex of the response surfaces. It is easier to understand by examining the contour plot in Fig. 4(a) that the change in the pin profiles are slightly more sensitive to the change in corrosion rate than to the change in rotational speed. Fig. 4(b) exhibits an almost circular contour, which suggests independence of factor effects, namely pin profile and welding speed, rotational speed of 1200 rpm and axial force of 12 KN. When at rotational speed of approximately 1200 rpm and a welding speed of 800 mm/min, it is slightly more sensitive to the change in corrosion rate, as illustrated in Fig. 4(c).

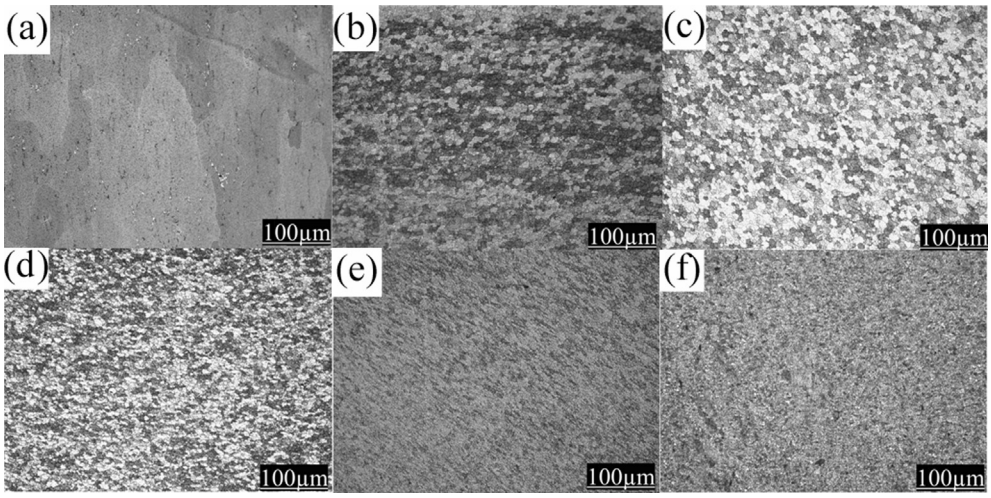

Fig. 6. Optical micrographs of AA2219 FSWelds of Nugget Zone (a) Base metal (b) Conical tool (c) Triangle tool (d) Square tool (e) Pentagon tool and (f) Hexagon tool.

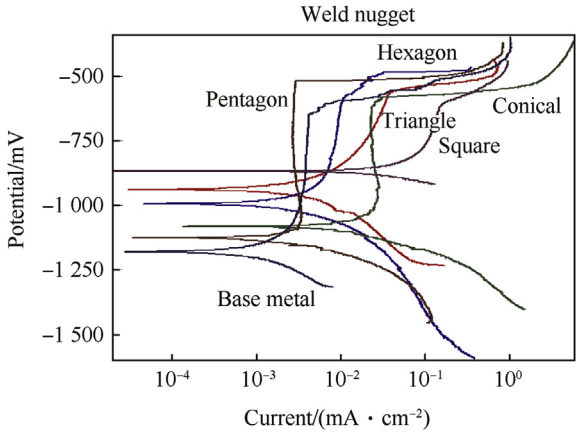

Fig. 7. Potentio-dynamic polarization curves of AA2219 FS welds prepared by five tool pin profiles.

The corrosion rate is more sensitive to the change in welding speed than to the change in rotational speed at an axial force of 12 KN for a square pin profile. An interaction effect of rotational speed and welding speed on the corrosion rate also exists, which is evidenced by the contour plot in Fig. 4(d). From the contour plot shown in Fig. 4(e), it is inferred that the corrosion rate is more sensitive to change in axial force than to the changes in rotational speed and welding speed when a square pin profile is used. There seems to be a pronounced interaction effect of axial force and rotational speed on corrosion rate when a square pin profile is used at a welding speed of 800 mm/min. The contour plot shown in Fig. 4(f) clearly demonstrates that the influence of axial force on corrosion rate is greater than that of welding speed at rotational speed of 1200 rpm for a square profile pin. The interaction effect between the factors is also evidenced.

The following inferences can be made from the contour plots and response surfaces. Of the five pin profiles used, the hexagon pin profile is more sensitive to corrosion rate at an optimum welding speed and axial force. Interaction effects among the factors of rotational speed and axial force, axial force and welding speed, and rotational speed and welding speed exist, and these interactions are more pronounced when a hexagon pin profile is used, which is evidenced and exhibited in the contour plots. The test results of corrosion current (I_{Corr}) and Corrosion resistance (E_{pit}) for the joints fabricated at lower and higher rotational speeds are given in Table 5. The maximum corrosion rate is obtained from the response surface and contour plots by using a hexagon pin profile with welding speed of 880.25 mm/min, a rotational speed of 1310 rpm and an axial force of 12.3 KN, assuming any two factors at optimum levels, as obtained from the simulated annealing algorithm method.

4.3. Effect of rotational speed

The joints fabricated at the lower and higher rotational speeds of 1000 rpm and 1400 rpm exhibited inferior corrosion properties. The corrosion testing results like corrosion current (I_{Corr}) and Corrosion resistance (E_{pit}) for the joints fabricated at lower and higher rotational speeds are given in Table 5. The corrosion resistance at 1000 rpm is more positive (−557 mV) than those at other rotational speeds, as shown in Table 3.

Table 5
Corrosion current values of welds with different parameters.

	Rotational speed (1400 rpm)	Rotational speed (1000 rpm)	Axial force (16 kN)	Axial force (8 kN)	Welding speed /(1000 mm·min^{-1})	Welding speed /(600 mm·min^{-1})
Corrosion current (I_{Corr})/(mA·cm^{-2})	0.0238832	0.1817653	0.0024928	0.0563769	0.0337123	0.0082865
E_{pit}/(mV)	−618	−557	−610	−591	−615	−558

4.4. Effect of welding speed

The corrosion testing results like corrosion current (I_{Corr}) and Corrosion resistance (E_{pit}) for the joints fabricated at lower and higher welding speeds are given in Table 5. The joints fabricated at a welding speed of 600 mm/min show corrosion properties superior to those of the other joints, at the corrosion resistance at this speed is more positive (−551 mV) than those at other welding speeds, as shown in Table 3.

4.5. Effect of axial force

Apparent variations in corrosion properties were found in the joints fabricated at lower and higher axial forces of 10 KN and 16 KN compared to the joints fabricated at axial force of 8 KN. The corrosion test results like corrosion current (I_{Corr}) and Corrosion resistance (E_{pit}) for the joints fabricated at lower and higher axial forces are given in Table 5. The corrosion property of joint fabricated at axial force of 8 KN is superior to those of the other joints, and its corrosion resistance (−558 mV) is more positive at an axial force of 8 KN than at other forces, as shown in Table 3.

5. Conclusions

1) The results indicate that the shape of the pin has a significant effect on the joint structure and the corrosion properties. The best quality weld was acquired using hexagon tool profile.
2) A mathematical model was developed to predict the corrosion resistances of friction stir welded AA2219 aluminium alloy joints with 95% of confidence level. The model was developed by incorporating the welding parameters and tool profiles using statistical tools, such as design of experiments and regression analysis.
3) The simulated annealing algorithm was used to optimize the friction stir welding parameters and tool profiles to attain maximum tensile corrosion resistance in the welded joints. The optimized values closely match the experimentally determined values. Response graphs and contour plots were drawn to study the interaction effect of welding parameters and tool profiles on the corrosion resistance of friction stir welded joints of AA2219 aluminium alloy.

Acknowledgements

The authors would like to thank Dr. A. Ghokale, Director, Defence Metallurgical Research Laboratory, and Hyderabad, India for his continued encouragement and permission to publish this work.

References

[1] Thomas WM, Nicholas ED, Needham JC, Murch MG, Temple Smith P, Dawas CJ. Int. Patent Appl. No. PCT/GB92/02203 and GB Patent Appl.9125978.8, Dec. 1991; U.S Oct. 1995: Patent Appl.No.5460317.
[2] Nandan R, DebRoy T, Bhadeshia HKDH. Recent advances in friction-stir welding. Process, weldment structure and properties. Prog Mater Sci 2008;53:980−1023.
[3] Sato YS, Kokowa H, Enomoto Masatoshi, Jogan Shigetoshi. Microstructural evolution of 6063 aluminum during friction-stir welding. Metall Mater Trans A 1999;30A:2429−37.
[4] Xu S, Deng X, Reynolds AP, Seidel TU. Finite element simulation of material flow in friction stir welding. Sci Technol Weld Join 2001;6(3):191−3.
[5] Threadgill PL, Leonard AJ, Shercliff HR, Withers PJ. Friction stir welding of aluminium alloys. Int Mater Rev 2009;54(2):49−93.
[6] Mishra RS, Ma ZY. Friction stir welding and processing. Mater Sci Eng 2005;50:1−78.
[7] Colegrove PA, Shercliff HR, Zettler R. Model for predicting heat generation and temperature in friction stir welding from the material properties. Sci Technol Weld Join 2007;12(4):284−97.
[8] Fratini L, Buffa G, Palmeri D, Hua J, Shivpuri R. Material flow in FSW of AA7075−T6 butt joints: numerical simulations and experimental verifications. Sci Technol Weld Join 2006;11(4):412−21.
[9] Yan Junhui, Sutton MA, Reynolds AP. Process−structure−property relationships for nugget and heat affected zone regions of AA2524−T351 friction stir welds. Sci Technol Weld Join 2005;10(6):725−36.
[10] Mukherjee S, Ghosh AK. Flow visualization and estimation of strain and strain-rate during friction stir process. Mater Sci Eng A 2010;527(20):5130−5.
[11] Nicholas ED, Thomas WM. A review of friction processes for aerospace applications. Int J Mater Prod Technol 1998;13(1−2):45−55.
[12] Samar Jyoti Kalita. Microstructure and corrosion properties of diode laser melted friction stir weld of aluminum alloy 2024 T351. Appl Surf Sci 2011;257(9):3985−97.
[13] Shigematsu I, Known YJ, Suzuki K, Imai T, Saito N. Joining of 5083 and 6061 aluminum alloys by friction stir welding. J Mater Sci Lett 2003;22(5):353−6.
[14] Mahoney M, Rhodes C, Flintoff J, Bingel W, Spurling R. Properties of friction-stir-welded 7075 T651 aluminium. Metall Mater Trans A 1998;29(7):1955−64.
[15] Arora A, De A, Deb Roy T. Towards optimum friction stir welding tool shoulder diameter. Scr Mater 2011;64(1):9−12.
[16] Cui GR, Ma ZY, Li SX. Periodical plastic low pattern in friction stir processed Al−Mg alloy. Scr Mater 2008;58:1082−5.
[17] Akinlabi Esther T, Anthony Andrews, Akinlabi Stephen A. Effects of processing parameters on corrosion properties of dissimilar friction stir welds of aluminium and copper. Trans Nonferrous Metals Soc China 2014;24(5):1323−30.
[18] Friggard O, Grong O, Bjorneklett B, Middling OT. In: Proc. 1st Int. Symp. on Friction Stir Welding., Thousand Oaks, CA, USA. TWI; June 1999.
[19] Zhao YH, Lin SB, Wu Lin, Qu FX. The influence of pin geometry on bonding and mechanical properties in friction stir weld 2014 Al alloy. Mater Lett 2005;59(23):2948−52.
[20] Thomas WM, Johnson KI, Wiesner CS. Friction stir welding − recent developments in tool and process technologies. Adv Eng Mater 2003;5:485−90.
[21] Flores OV. Scr Mater 1998;38:703.
[22] Bagheri Hariri Mohiedin, Gholami Shiri Sajad, Yaghoubinezhad Yadollah, Mohammadi Rahvard Masoud. The optimum combination of tool rotation rate and traveling speed for obtaining the preferable corrosion behavior and mechanical properties of friction stir welded AA5052 aluminum alloy. Mater Design 2013;50:620−34.
[23] Liu HJ, Fuji H. Sci Technol Welding J 2003;8:450.
[24] Liu HJ, Chen YC, Feng JC. Scr Mater 2006;55:231.
[25] Box GEP, Hunter WH, Hunter JS. Statistics for Experiments. New York: John Wiley Publications; 1978.
[26] Miller I, Freund JE, Johnson RA. Probability and Statistics for Engineers. 5 Pvt. Ltd. New Delhi: Prentice of Hall of India; 1999.
[27] Montgomery DC. Design and analysis of experiments. New York: John Wiley & Sons; 2001.
[28] McMullen PR, Frozier GV. An simulated annealing approach to mixed model sequencing with multiple objectives. IIE Trans 2000;32:679−86.